Available online at www.sciencedirect.com
SCIENCE DIRECT
Carbohydrate Polymers 65 (2006) 64–74
Carbohydrate Polymers
www.elsevier.com/locate/carbpol

Atomic force microscopy of pea starch: Granule architecture of the *rug3-a*, *rug4-b*, *rug5-a* and *lam-c* mutants

Michael J. Ridout [a], Mary L. Parker [a], Cliff L. Hedley [b], Tatiana Y. Bogracheva [b], Victor J. Morris [a,*]

[a] *Institute of Food Research, Norwich Research Park, Colney, Norwich NR4 7UA, UK*
[b] *John Innes Centre, Norwich Research Park, Colney, Norwich NR4 7UH, UK*

Received 16 November 2005; accepted 14 December 2005
Available online 8 February 2006

Abstract

Atomic force microscopy has been used to visualise the internal structures of sectioned, encased starch granules isolated from near-isogenic pea starch mutants (*rug3-a*, *rug4-b*, *rug5-a*, and *lam-c*). A mutation at the locus *rug4* was found to have little effect on the granule ultrastructure. However, mutations at *rug3* and *lam*, which give rise to low-amylose starches, led to granules that showed banding (growth rings) in which individual blocklets could not easily be seen. High-amylose (*rug5*) mutants formed granules ranging in shape from simple ellipsoids through to quite complex, convoluted structures. The internal granule structure was found to be heterogeneous. In some regions, normal banding was visible and the underlying 'hard' blocklets were embedded in a 'soft' matrix. In other regions of the granule, the banding structure was absent and the matrix in which the blocklets are embedded contained a fine hard network structure. It is proposed that this fine, hard structure is due to the presence of a crystalline amylose network.

Keywords: Starch granule structure; Growth rings; Atomic force microscopy; Near-isogenic pea starch mutants

1. Introduction

The atomic force microscope (AFM) provides a new method for probing the ultrastructure of starch granules. To obtain AFM images of the internal structure of starch granules it is necessary to prepare samples with relatively flat surfaces, which are best obtained by the use of sectioned, embedded granules (Baker, Miles, & Helbert, 2001; Ridout, Gunning, Wilson, Parker, & Morris, 2002). It has been shown that the choice of embedding resin influences the contrast seen in the AFM images and may even introduce artefacts into the images (Ridout et al., 2002). However, through the use of a non-penetrating resin to encase, rather than embed the granules, it is possible to obtain routinely images of starch ultrastructure under near-native conditions. Recently, it has been demonstrated that the contrast in AFM images of encased starch material results from the selective, localised absorption of water within the encased starch granule (Ridout, Parker, Hedley, Bogracheva, & Morris, 2004). The ability to map the local hardness of the exposed face of the granule, together with the localised wetting and swelling of sections of this face of the granule, permits the observation of the localisation of glassy, crystalline and amorphous (rubbery) material within the starch granule. The images obtained provide support for the blocklet model of starch granule structure (Gallant, Bouchet, & Baldwin, 1997). On the basis of this model, it has been proposed that the AFM images of wild-type starch support the proposed localised distribution of the majority of the amylose and amylopectin within the granules (Ridout et al., 2004).

Published AFM studies of starch granule surfaces (Baldwin, Adler, Davies, & Melia, 1998; Szymonska & Krok, 2003; Szymonska, Krok, & Tomasik, 2000) and of the internal structure (Baker et al., 2001; Ohtani, Yoshino, Ushiki, Hagiwara, & Mackawa, 2000a,b; Ridout et al., 2002; Ridout, Parker, Hedley, Bogracheva, & Morris, 2003) of starch granules have added weight to the idea of blocklet structures. Detailed AFM investigations of the internal structure of pea starch granules (Ridout et al., 2002) have suggested that the blocklets are distributed uniformly within the granules and that the so-called 'amorphous growth rings' arise from localised defects in the growth of the granules. It has been proposed that such defects may arise due to reduced levels of deposition of

* Corresponding author. Tel.: +44 1603 255271; fax: +44 1603 507723.
E-mail address: vic.morris@bbsrc.ac.uk (V.J. Morris).

0144-8617/$ - see front matter © 2006 Elsevier Ltd. All rights reserved.
doi:10.1016/j.carbpol.2005.12.016

Table 1
Isogenic pea starch mutants

Loci	Mutated enzyme	Function
r	Starch branching enzyme A	Amylopectin synthesis
rb	ADP glucose pyrophosphorylase	Substrate supply
rug3	Phosphoglucomutase	Substrate supply
rug4	Sucrose synthase	Substrate supply
rug5	Granule-bound starch synthase II (GBSS II)	Amylopectin synthesis
lam	Starch synthase I	Amylose synthesis

amylose within specific regions of the granule (Ridout et al., 2002).

Further, progress has been achieved by studying a family of pea starch mutants (Ridout et al., 2002). These mutants are known to be affected at specific steps in the starch biosynthetic pathway and have been back-crossed into a common background (Bogracheva, Wang, Wang, & Hedley, 2002; Denyer et al., 1995; Harrison, Hedley, & Wang, 1998; Hedley et al., 1995; Hylton & Smith, 1992; Wang et al., 1994). They can be regarded as near isogenic, apart from those genes present at the loci where mutations have been identified. This collection of mutants can be divided into two classes. Firstly, those mutants involving enzymes (Table 1) that determine the supply of substrate during starch biosynthesis (Wang, Bogracheva, & Hedley, 1998). Secondly, mutants in genes that encodes enzymes that are involved directly in the synthesis of starch polysaccharides (Wang et al., 1998) (Table 1). The mutations provide a means of varying the amylose-to amylopectin ratio and for observing the effect of such changes on the structure and function of pea starch (Bogracheva et al., 1999).

The *rb* mutation was found to lead to only small modifications in the ultrastructure and functional properties of the granule (Ridout et al., 2003). However, the *r* mutation, Which leads to a high-amylose starch caused substantial changes in granule structure and functionality (Bogracheva et al., 1999; Ridout et al., 2003). The *r* mutation was shown to give rise to the formation of a new and unexpected hard, fine network permeating throughout the entire granule, primarily contained within the matrix region surrounding the blocklets (Ridout et al., 2003). The presence of this network was used to account for the fragility of the granules. We have suggested (Ridout et al., 2003, 2004), on the basis of the Gallant and co-workers view (Gallant et al., 1997) of granular structure, that this hard, fine network is produced by crystallisation of a small fraction of the amylose within the matrix surrounding the blocklets. The presence of such an amylose network would account for the reduced swelling of the granules and the broadened gelatinisation behaviour. Amylose crystallisation within the granule is consistent with the fact that, although the wild-type parent is a C-type starch, the *r* mutant is B-type. Lintnerisation of the *r* mutant starch reveals that the crystalline regions within the granule contain a new higher-molecular weight population of amylosic chains. This amylosic fraction was not observed in the chain profiles of the de-branched amylopectin extracted from either the *r* mutant or the wild-type parent starch. High-amylose starches contain amylose and amylopectin but will also contain additional levels of intermediate material, varying between lightly branched amyloses and amylopectins with additional long branches. In the *r* mutant such intermediate material may contribute to the formation of the new network structure. The double mutant *rrb* was found to possess structural features related to both the *r* and the *rb* mutants (Ridout et al., 2003). This was consistent with the functional behaviour of the double mutant; the properties of which were found to be intermediate between those of the single mutants.

In this article, we describe further studies of near-isogenic pea starch mutants: the 'substrate supply' mutants *rug3-a* and *rug4-b*, and the 'polymer' mutants *lam-c* and *rug5-a*. The aim is to identify and define differences and similarities between mutants, rather than to generate the highest resolution images.

2. Materials and methods

The samples of pea starch were extracted from the seeds of the wild-type parental line and from a series of mutants (*rug3-a*, *rug4-b*, *rug5-a*, and *lam-c*), that are near-isogenic to the wild-type parent, using the methods described by Bogracheva and co-workers (Bogracheva et al., 1999, 2002; Ridout et al., 2004).

The *rug3-a* and *rug5-a* samples were air-classified and the coarse fraction used for isolation of the starch.

Samples for AFM studies were prepared by encasing the air-dried starch in rapid-set Araldite (Bostik Ltd) and cutting sections onto water with glass knives using an ultramicrotome (Ultracut E, Reichert-Jung). The wetting of the underside of the section generates contrast in the AFM images. It also ensures that any amylose leaked from the exposed lower face is washed away before depositing the section onto the glass substrate.

AFM images were obtained on a Thermomicroscopes Lumina combined AFM/SNOM system. The sections were scanned in air using the 'dry-scanner attachment'. Topographic and error signal mode images were obtained by scanning the sections in the dc contact mode using silicon nitride cantilevers with a nominal force constant of 0.38 $N\,m^{-1}$. The scan rate was generally between 2.0 and 2.5 Hz. The stiffness of the exposed faces of the granules was mapped in the force modulation mode. The cantilevers were driven at a frequency of 5 kHz into the sample surface with typical amplitudes of 4.0 nm.

In general, the samples of encased starch will contain 10–20 granules. For each mutant about 60 granules will be examined. If there is marked variation between granules then examples are shown of each form. For each mutant typical images of single granules have been chosen and displayed. The images selected are those cut through the centre of the granule where the hilum is visible. Higher resolution images of starch ultrastructure are typical of those seen throughout the granule unless otherwise stated in the text.

3. Results and discussion

In previous AFM studies of cut faces of blocks of encased starch, or sections of starch granules encased in rapid-set Araldite, it has been shown (Ridout et al., 2004) that this technique provides reproducible images of the internal structure of the near-native starch granule. The images presented in this article were obtained on sectioned, encased starch. We have shown in previous papers (Ridout et al., 2003, 2004) that the contrast in the AFM images is due to selective absorption of water within the sections, leading to preferential swelling of the amorphous regions of the sectioned granule.

3.1. The wild-type pea starch

The types of low- and higher resolution images obtained of the wild-type pea starch (Ridout et al., 2003, 2004) are illustrated schematically in Fig. 1. The exposed face of the granule shows that the growth-ring structure appears as a series of concentric bands. The internal structure of starch granules is generally considered to consist of crystalline and amorphous growth rings (Gallant et al., 1997). We believe the bright and dark bands seen in the AFM images correspond to what are normally called the 'crystalline' and 'amorphous' growth rings. The dark unswollen bands were found to be discontinuous and consisted of a series of unswollen patches. At higher resolution no internal structure could be observed within these unswollen patches. The bright swollen bands and the swollen regions between patches in the dark bands contained a substructure. At higher resolution the AFM images revealed arrays of what appear to be prolate ellipsoidal objects, aligned almost radially and contained within a featureless matrix region. This structure is shown in an insert in Fig. 1 and schematically in Fig. 2. On the basis of the Gallant and co-workers description (Gallant et al., 1997) of starch granules, at least for the wild-type parent, the ellipsoidal structures are considered to be largely amylopectin-based blocklets, immersed in a swollen amorphous largely amylose-based matrix. The schematic diagrams (Figs. 1 and 2) show that the blocklet structures are contained throughout the granule. The banding appears because there are small regions distributed within the granule, which do not swell. These regions pin down the structure leading to variations in the height and hardness of the exposed face of the granule. This is the origin of the banding in the AFM images. The effect of small non-swelling patches is illustrated schematically in Fig. 2. The patches pin down the structure modulating variations in hardness and height of the exposed face of the granule. The structures seen in the AFM images correlate with those seen by other forms of microscopy. This is because the swollen regions are more likely to accumulate dye or stain, or to be degraded by acid or enzymes. On the basis of the Gallant and co-workers (1997) model it has been suggested that the unswollen patches in the dark bands arise due to reduced deposition of amylose during the growth of the granule structure (Ridout et al., 2003, 2004). As we have noted previously (Ridout et al., 2003, 2004) both the bright and dark bands contain blocklets and hence both are partially crystalline. Therefore, we believe that the terms 'crystalline and amorphous' growth rings are poor and inappropriate descriptions of the structure and that it is preferable simply to refer to bright and dark bands. Gallant et al. (1997) have suggested that

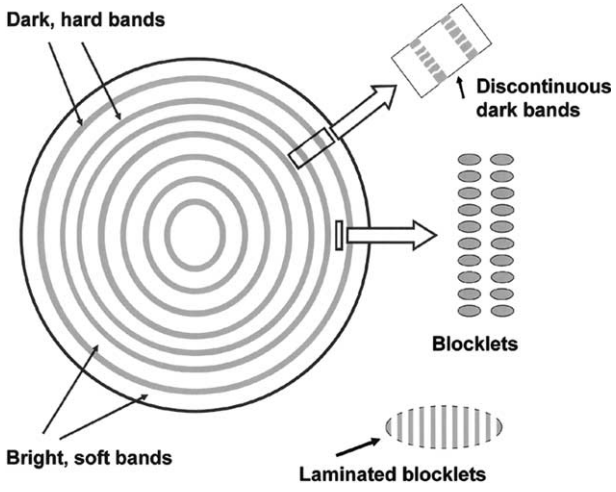

Fig. 1. A schematic picture of the internal structure of sectioned, encased starch granules, as revealed by AFM. The substructure seen within the swollen regions of the granule and the discontinuity of the dark bands are illustrated in the inserts. The substructure of the bright bands is believed to be largely amylopectin-based blocklets immersed in an amorphous matrix consisting largely of amylose. The laminated nature (crystalline and amorphous regions) of the blocklets, as revealed by transmission electron microscopy (Gallant et al., 1997), is shown schematically.

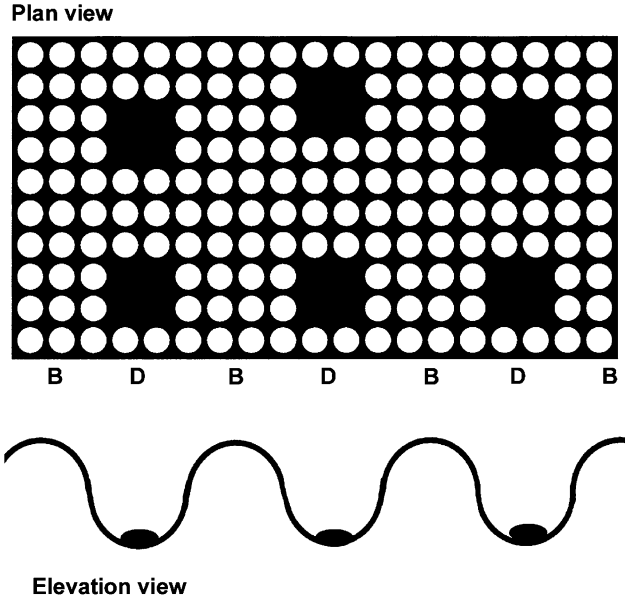

Fig. 2. A schematic picture showing the blocklets embedded in a swollen largely amylose-based matrix. The swelling leads to differences in hardness and height, which give rise to the banded structure known as growth rings. The dark bands arise because of the presence of patches or defects that do not swell and pin the exposed face of the granule. These patches lie at the bottom of the Undulations induced by the absorption of water as shown in the lower diagram. The bright and dark bands are marked 'B' and 'D', respectively, for both the plan and elevation. In the plan, the blocklets are shown as white objects embedded in a black matrix.

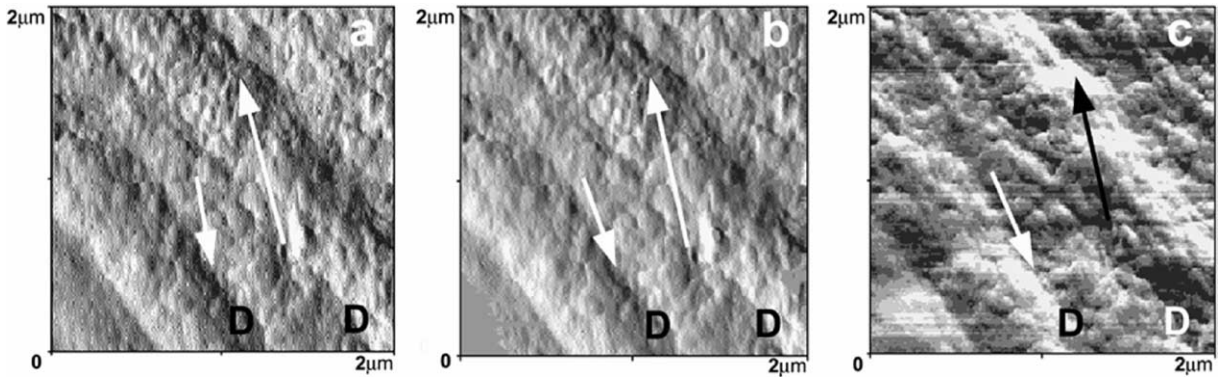

Fig. 3. AFM images of sectioned, encased wild-type pea starch granules: the scan size is 2×2 μm; (a) left-shaded topography image; (b) error signal mode image; (c) force modulation image. Patches forming the discontinuous dark bands are indicated by arrows and exist within dark bands labelled 'D'. These patches appear bright in the force modulation image.

the blocklets may be composed of single amylopectin molecules.

Fig. 3 shows higher resolution AFM data on the exposed face of a sectioned encased wild-type pea starch granule. The image shown in Fig. 3(a) is a left-shaded topography image showing the growth rings and the blocklet structure within the bright, swollen bands. The dark bands are composed of patches of unswollen material (labelled D and arrowed in Fig. 3). The image shown in Fig. 3(b) is an error signal mode image. The error signal mode of imaging acts as a filter that highlights the detailed surface structure and this is useful for displaying the fine detail of the structure of rough samples such as encased starch granules (Ridout et al., 2004). Visually, the images are similar and it is more convenient to display images as error signal mode images. Fig. 3(c) shows a force modulation AFM image of the same region of the exposed face of the granule. In the force modulation mode, the contrast depends on the initial slope of the force-distance curve generated by the oscillating probe (Ridout et al., 2004). Thus, the image displays the hardness of the sample surface. Bright regions in the force modulation images indicate harder regions of the sample surface. The patches indicated by arrows, marked 'D' in Fig. 3, appear bright relative to the surrounding matrix region in Fig. 3(c), consistent with the idea that these are unswollen hard regions of the exposed surface of the granule.

The ellipsoidal blocklets are easier to see in the force modulation image where they appear brighter relative to the surrounding matrix region. The blocklets are considered to be composed of the crystalline lamellae, formed from the amylopectin branches, interspersed by amorphous regions (shown in the insert to Fig. 1). In previous discussions on the origin of contrast in AFM images, we have proposed (Ridout et al., 2004) that the amorphous amylose matrix surrounding the blocklets swells more than the blocklets themselves, which therefore appear as harder objects in a softer matrix.

An understanding of the origins of contrast in the AFM images is important in comparing the present results with published transmission electron microscopy (TEM) data (Gallant et al., 1997). The classic TEM images of blocklets in sectioned maize starch were obtained by generating contrast using the PATAg (periodic acid, thiosemicarbazide, silver) reaction (Gallant et al., 1997). Crystalline regions of the granule are oxidized at a slower rate than amorphous regions and thus, if the reactions are carried out under weak oxidation conditions, silver ions will be preferentially accumulated and stain the amorphous regions. The largely unstained blocklets then appear as bright objects in a dark background, due to the selective staining of the sectioned material. The AFM data presented above confirms this picture with the more-crystalline blocklets appearing as hard objects in a softer, swollen matrix material.

Gallant et al. (1997) have revived and redefined the 'blocklet model' of starch ultrastructure, in which blocklets are considered to be essentially parcels of partially crystalline amylopectin contained within the growth ring structure of the starch granule. The crystalline component of the blocklets arises from the ordering of short branches of the amylopectin molecules. This laminated structure within blocklets (see insert in Fig. 1) has been observed by TEM but is difficult to resolve by AFM on unmodified samples. The elegant cluster model of starch structure (Buleon, Colonna, Planchot, & Ball, 1998a,b; Gallant et al., 1997), and the refinement in terms of the side-chain liquid-crystalline model of starch (Waigh, Kato, Donald, Gidley, & Reikel, 2000; Waigh, Perry, Reikel, Gidley, & Donald, 1998), describes the detailed intra-blocklet structure. In previous studies of isogenic pea starch mutants, it has been shown that the major changes in starch structure which gives rise to, and can be used to explain changes in starch functionality, occur at the inter-blocklet level of organization (Ridout et al., 2003, 2004).

3.2. The rug3-a pea starch mutant

The low-resolution AFM images show that the *rug3-a* pea starch granules are similar in shape to the wild-type parent. A typical topographical image (Fig. 4(a)) shows that wetting during sectioning has led to swelling of the material out of the section leading to a marked variation in height (∼800 nm) across the granule structure. The swelling discussed here is not necessarily the same as the normal swelling behaviour of intact granules. Sectioning exposes faces of the interior of the granule

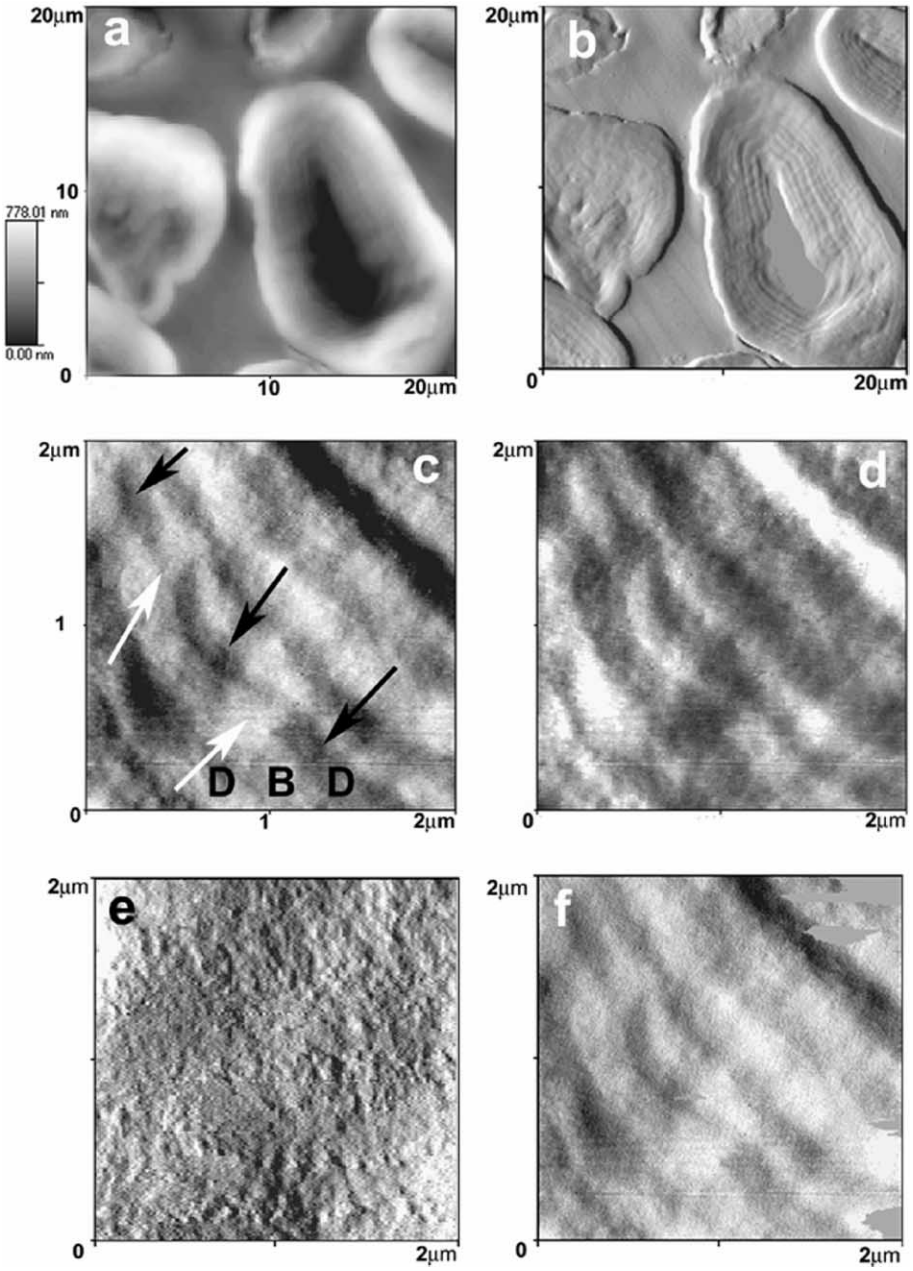

Fig. 4. AFM images of sectioned, encased *rug3-a* pea starch granules: (a) topography image, scan size 20×20 μm; (b) left-shading of the topography image shown in Fig. 3(a), scan size 20×20 μm; (c) higher resolution error signal mode image of a region close to the edge of an encased starch granule, in a region where the growth ring structure is well defined, scan size 2×2 μm; (d) force modulation image of the region shown in (c) scan size 2×2 μm; (e) higher resolution image of the interior of the granule in a region close to the centre of the granule, where the growth ring structure is less distinct, scan size 2×2 μm; (f) left-shaded high-resolution topography image of the region shown in c and d, scan size 2×2 μm. The black arrows indicate discontinuous unswollen patches and the white arrows show the interlinking swollen regions. Bright and dark bands are marked 'B' and 'D', respectively.

which, when in contact with water during sectioning, can absorb water and expand without constraint.

The central regions of the granules are dark implying that swelling is more noticeable at the outer extremities of the granule. One explanation for this effect could be that the centre of the granule is different in structure, and swells less than regions at the edge of the granule. This effect is the same as that observed for the wild-type parent (Ridout et al., 2003, 2004) and we have previously suggested that the whole of the section expands whilst in contact with water (Ridout et al., 2004). Then, when the section is deposited onto glass substrates and allowed to equilibriate in air, the swollen region collapses, with the portion at the centre collapsing more than the regions near to the edges of the granule (Ridout et al., 2004). This explanation is essentially that proposed to explain the folding artefacts commonly seen in TEM studies of thin sections of embedded starch (Hood & Liboff, 1983).

The shaded topography image (Fig. 4b) clearly displays the growth ring structure of the granule. As discussed in detail for the wild-type material (Ridout et al., 2004), the contrast in the

images is due to the selective swelling of the sectioned material. This is confirmed in the higher resolution error signal mode (Fig. 4(c)) and force modulation (Fig. 4(d)) images of the granule. The bright bands in the error signal mode image (Fig. 4(c)), corresponding to swollen regions in the topography image, are dark in the force modulation image (Fig. 4(d)). Similarly, the dark patches (marked with black arrows in Fig. 4(c)) defining the discontinuous unswollen dark bands are bright (stiff) in the force modulation image (Fig. 4(d)). These discontinuities are essentially the same as those observed previously for the wild-type parent and the nature and possible origin of these defects in the granule structure have been discussed in detail elsewhere (Ridout et al., 2004). At this higher resolution, the error signal mode images from near the centre of the granule, where the growth ring structure is less distinct (Fig. 4(e)), and the left-shaded topography image near the edge of the granule (Fig. 4(f)), reveal some evidence for a mottled appearance which could be consistent with an underlying blocklet structure. However, the contrast is very poor and any blocklets are very difficult to see or characterise, although the few spheroidal structures clearly visible are smaller in size than the blocklets seen in the images of the wild-type parent (Fig. 3).

3.3. The rug4-b pea starch mutant

The *rug4-b* pea starch granules are similar in shape to the wild-type parent. The topography image (Fig. 5(a)) shows the variation in height across the swollen section with the central dark region. The large variation in height obscures the details of the internal structure of the granule. The shaded topography image (Fig. 5(b)) reveals the growth ring structure of the granule.

At higher-resolution (Fig. 6) it can be seen that the bright and dark bands arise due to selective swelling of regions of the granule. The bright bands seen in the left-shaded topography image (Fig. 6(a) and (d)) and the equivalent error signal mode image (Fig. 6(b) and (e)) are dark in the force modulation image (Fig. 6(c) and (f)) confirming that they are selectively swollen regions within the granule. The dark bands (Fig. 6(a), (b), (d) and (e)) are discontinuous, and the dark patches are bright in the force modulation image (examples are indicated by the white arrows in Fig. 6(b) and (c)), indicating that these are unswollen regions of the granule. No fine structure is visible within these unswollen patches. The nature of these discontinuities is similar to those seen in the wild-type parent and their origin has been discussed in detail elsewhere (Ridout et al., 2003, 2004). However, throughout the remainder of the granule the blocklet structure is visible in the shaded topography (Fig. 6(a) and (d)), error signal mode (Fig. 6(b) and (e)) and force modulation (Fig. 6(c) and (f)) images. The brightness of the blocklets in the force modulation images (Fig. 6(c) and (f)) is consistent with hard objects embedded in a softer matrix material.

Previous work on the *rb* mutant, and the present studies on the *rug4-b* mutant, suggest that these mutations do not lead to significant changes in the architecture of the starch granule. However, the major effect of these substrate mutations seems to be on the amount of starch produced by the plant (Bogracheva, Davydova, Genin, & Hedley, 1995) and the ratio of the A and B crystallites within the granules. The wild-type pea starch is a C-type starch and it has been shown that the granule contains both A- and B-type crystals (Cairns, Bogracheva, Ring, Hedley, & Morris, 1997; Gernat, Radosta, Damaschun, & Schierbaum, 1990). The B-type crystals are located centrally and the A-type crystals peripherally within the granule (Bogracheva, Morris, Ring, & Hedley, 1998; Buleon, Gerard, Riekel, Vuong, & Chanzy, 1998). In this and previous studies (Ridout et al., 2003, 2004), we have not been able to observe any difference in size or shape of the blocklets which could be attributed to differences in the type of crystals found near the centre (B-type) or at the periphery of the granules (A-type). Where blocklets have been visible they are of the same size and shape throughout the granule for the wild-type parent, *rb*, and *rug4-b* mutants (Ridout et al., 2003, 2004). This is perhaps not surprising since the distinction between A- and B-type crystals depends on the inter-helix arrangement within the crystalline lamellae inside blocklets (Buleon et al., 1998a,b; Gallant et al., 1997).

The wild-type parent, the *rb* mutant, and *rug4-b* mutants show similar gelatinisation and bulk-swelling properties. In all cases, gelatinisation is characterised by a relatively sharp

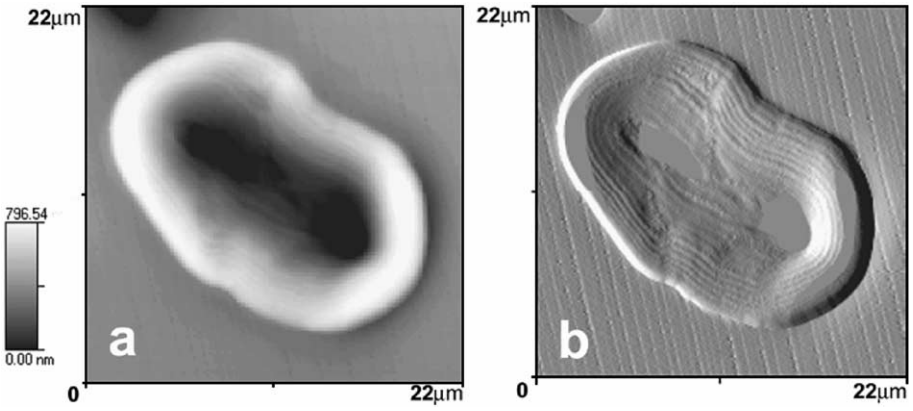

Fig. 5. AFM images of a typical sectioned, encased *rug4-b* pea starch granule: (a) topographical image, scan size 22×22 µm; (b) left-shaded topographical image, scan size 22×22 µm.

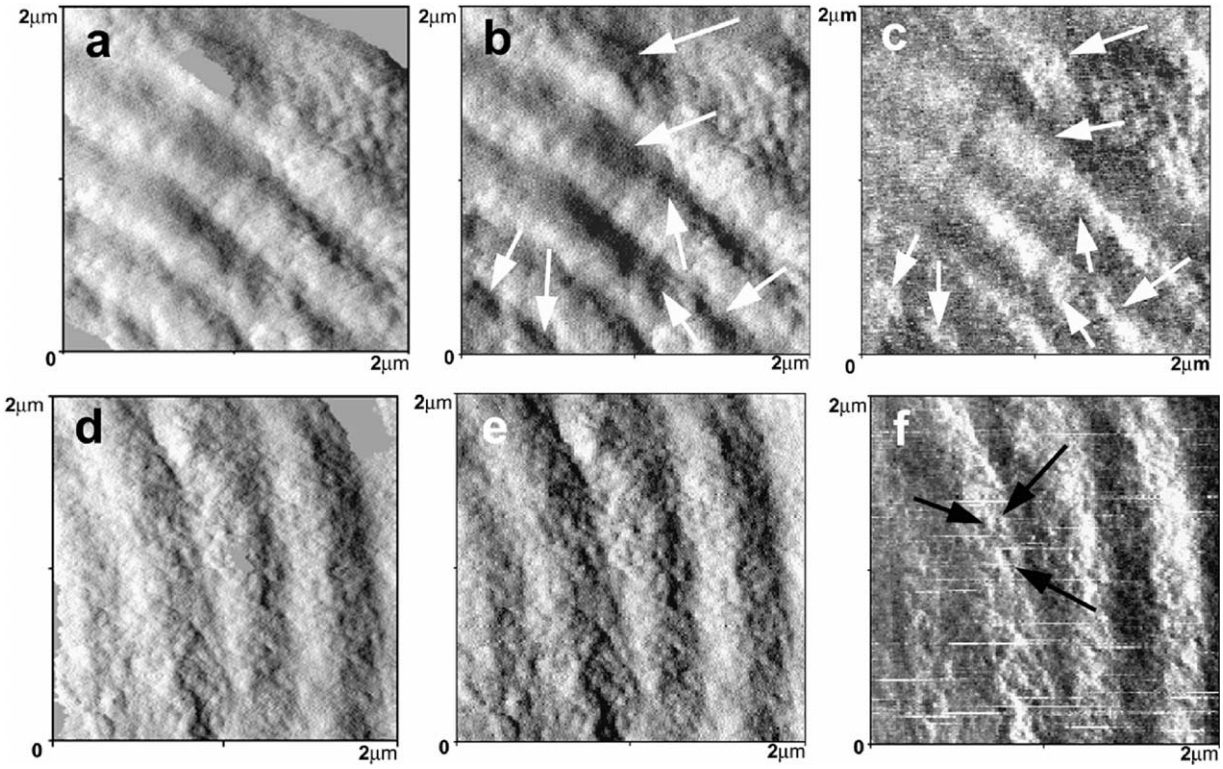

Fig. 6. AFM images of the interior of a sectioned, encased *rug4-b* pea starch granule: (a and d) left-shaded topography image, scan size 2×2 μm; (b and e) error signal mode image, scan size 2×2 μm; (c and f) force modulation image, scan size 2×2 μm. The white arrows indicate unswollen patches in the dark bands. The black arrows indicate the most prominent hard blocklets in a bright band.

endothermic peak (Bogracheva et al., 1999). Gelatinisation has been shown to involve disruption of the crystalline structure at the centre of the granule, which propagates outwards, accompanied by progressive swelling of the granule (Bogracheva et al., 1998, 2002). Differences in the proportions of A-type and B-type crystals in the granules may help account for the differences in peak gelatinisation temperatures. The gelatinisation of these mutants is discussed in detail elsewhere (Bogracheva et al., 1998, 2002).

In previous studies (Ridout et al., 2003, 2004) significant changes seen in the granule ultrastructure have been observed for the *r* mutant. Therefore, it is instructive to consider whether the other 'polymer' mutants *lam-c* and *rug5-a* show equally significant changes in granule structure.

3.4. The lam-c pea starch mutant

Data on the *lam-c* mutant is shown in Fig. 7. The topography image (Fig. 7(a)) is typical. The granules are ellipsoidal and similar in shape to the wild-type starch. Wetting has led to selective swelling of the granule, which is most apparent near the extremities of the starch granule.

At higher resolution the left-shaded topography image (Fig. 7(b)) shows the banded structure more clearly seen near the edges of the granule. At higher resolution the topography image (Fig. 7(c)) shows that the banded structure consists of bright (swollen) and dark bands and that the dark bands are discontinuous (Fig. 7(c) and (d)). The dark unswollen patches which define the dark bands are indicated by white arrows in Fig. 7(c). Left-shading has been used in Fig. 7(d) to try to reveal any substructure (blocklets) within the bands. As with the other low-amylose mutant *rug3-a*, no clearly defined blocklet structure can be seen.

In the *lam-c* mutant, the amylose content has been reduced from 35% to about 8%, but the level of crystallinity remains approximately the same (Bogracheva et al., 1999). Although the nature of the amorphous material is not clearly defined preferential swelling of localised amorphous regions within the granule will lead to the contrast in the images. The existence of bands (growth rings) and the patchy nature of the dark bands suggest that there are, as in the wild type parent, periodical fluctuations in the levels of crystalline material laid down in the dark and light bands within the granule. It was not possible to find any clear evidence for blocklet structures in any of the higher resolution images. One could argue that if, in the wild-type material, it is the localised swelling of an amylose matrix surrounding individual blocklets that reveals the blocklet structure, then it is perhaps not surprising that discrete blocklets are not seen in the *lam-c* and *rug3-a* mutants. However, the absence of any visible blocklet structure may also indicate that the overall relative spatial arrangement of the crystalline lamellae within the bands (growth rings) of the granule is completely different in low-amylose starches.

3.5. The rug5-a pea starch mutant

The structure of the *rug5-a* mutant starch granules is particularly interesting, because this mutant shows modified

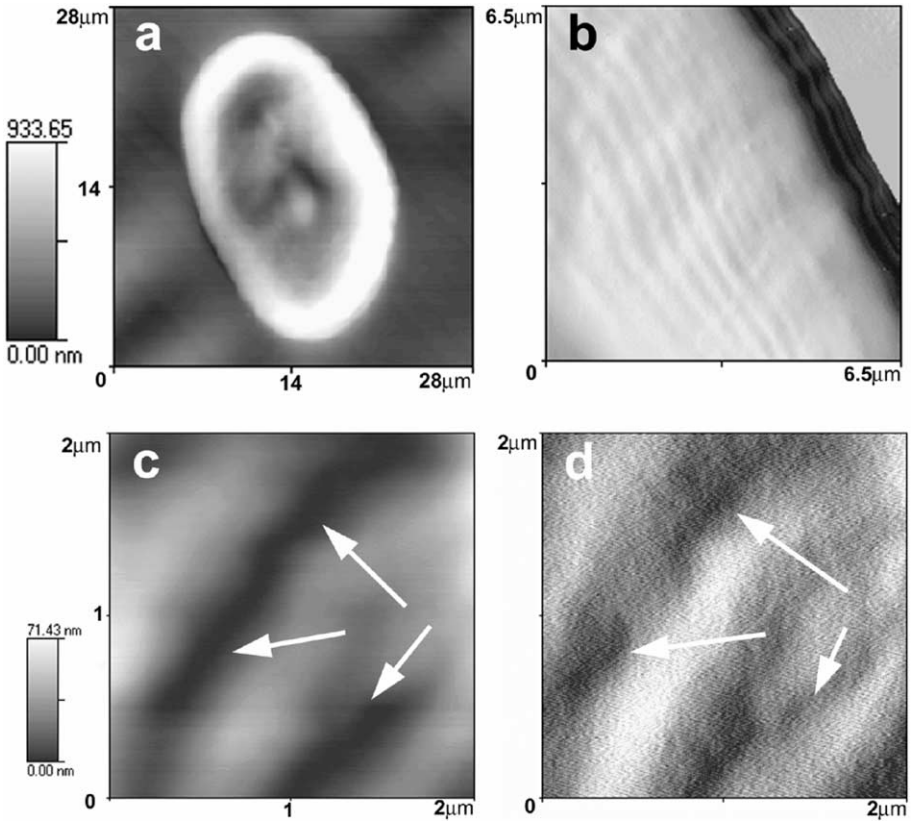

Fig. 7. AFM images of typical sectioned, encased *lam-c* mutant pea starch granules: (a) topography image, scan size 28×28 μm; (b) left-shaded topography image near the edge of a granule showing banding, scan size 6.5×6.5 μm; (c) topography image, scan size 2×2 μm; (d) left-shaded topography image, scan size 2×2 μm. The white arrows indicate unswollen patches that define the dark bands.

gelatinisation behaviour very similar to that of the *r* mutant (Bogracheva et al., 1999). Light microscope pictures of *rug5-a* mutant starch granules, imaged under crossed polarisers, show that the birefringent areas are randomly distributed throughout the granules (Hedley, Bogracheva, & Wang, 2002). This suggests that the crystalline regions are distributed in an Apparently non-ordered way throughout the granule. The topography images (Fig. 8(a) and (b)) show a range of shapes from a few simple ellipsoids through to quite complex convoluted structures. The overall height variation across the granules is quite large (∼1 μm). Most of the granules do not have a clearly recognisable centre or hilum, but the folding is more pronounced around the edges of the granules. The central regions are dark and lower in height. Once again this could imply variation of the structure and the subsequent swelling throughout the granules or, more likely, reflects collapse of the inner regions of the swollen structure, when the sections are deposited on to the glass microscope slides and stored under ambient conditions.

Because of the convoluted nature of the granule structure it is difficult to see growth rings or blocklets in these low-resolution images even after shading or through use of the error signal mode. The granules consist of two regions: rough regions showing significant height variations where

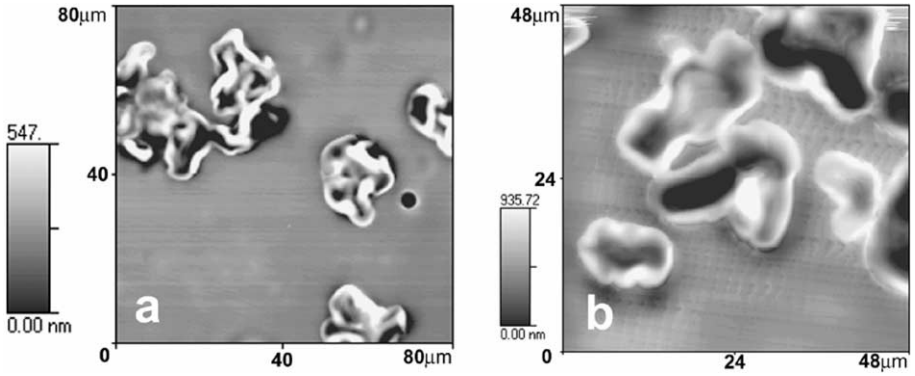

Fig. 8. AFM images of sectioned, encased *rug5-a* mutant pea starch granules: (a) topography image, scan size 80×80 μm; (b) topography image, scan size 40×40 μm.

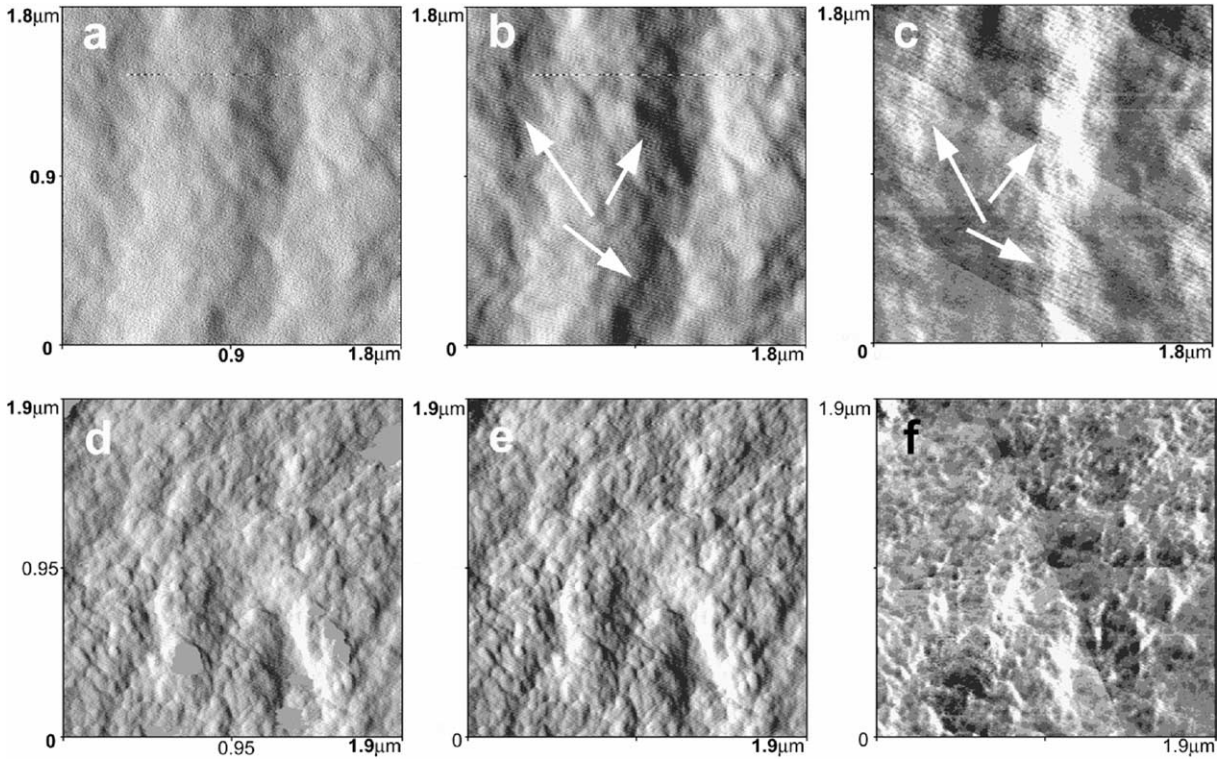

Fig. 9. AFM images of the interior of sectioned, encased *rug5-a* mutant pea starch granules: (a) topography image, scan size 1.8×1.8 μm; (b) error signal mode image, scan size 1.8×1.8 μm; (c) force modulation image, scan size 1.8×1.8 μm; (d) topographical image, scan size 1.9×1.9 μm; (e) left shaded topography image, scan size 1.9×1.9 μm; (f) error signal mode image, scan size 1.9×1.9 μm; (f) force modulation image, scan size 1.9×1.9 μm. Arrows indicate unswollen patches. The blocklets seen in 'e' appear as black holes in 'f' because they are surrounded by a harder matrix material.

banding can be seen and flat regions where no banding is seen.

The higher resolution images obtained from regions with banding are different from those obtained from regions where growth rings are absent (Fig. 9). Fig. 9(a)–(c) shows high-resolution images obtained near the extremity of a granule, in a region where growth rings are visible. The topography (Fig. 9(a)) and error signal (Fig. 9(b)) mode images show that the growth rings are bands of light (high) and dark (low) areas within the granule. The dark unswollen patches that define the dark bands are arrowed in Fig. 9(b). The equivalent force modulation image (Fig. 9(c)) suggests that the dark patches, seen in Fig. 9(a) and (b), are hard, bright (arrowed in Fig. 9(c)) in the force modulation image and the bright bands, seen in Fig. 9(a) and (b), are soft. This is consistent with the idea that the contrast is due to selective swelling of regions within the granule and that the dark bands (Fig. 9(a) and (b)) are discontinuous structures composed of localised patches of hard, unswollen material. In the regions of the granule, which do not show banding, the images are quite different (Fig. 9(d)–(f)). Although no bands are seen, the granules contain blocklets visible in the shaded-topography (Fig. 9(d)) and error signal mode (Fig. 9(e)) images. These regions of the granule are quite flat and the height variation across the image is about 55 nm. The force modulation (Fig. 9(f)) images show that the hardest regions within this part of the granule correspond to a hard, fine network structure contained within the matrix material surrounding the blocklets. The blocklets appear as black holes in a harder (bright) network. This is similar to the situation observed with the *r* mutant, where a hard, fine network structure was found to permeate throughout the entire granule (Ridout et al., 2003, 2004). It was suggested that the network arose due to a crystallisation of fraction of the amylose within the matrix (Ridout et al., 2003, 2004). In a similar fashion, we suggest that the present observations are also compatible with the formation of a crystalline amylose network.

In order to explain the enhanced hardness of the matrix material, it is suggested that in the *rug5-a* mutant, the generation of excess amylose (up from 35 to 43%) (Bogracheva et al., 1999), leads to crystallisation of a fraction of the material forming the hard matrix. Support for this suggestion comes from lintnerisation studies of the granules (Bogracheva et al., 1999). For the *rug5-a* mutant, the profile of amylosic chains contained within the crystalline regions is very broad (Bogracheva et al., 1999), and much broader than the branch-length distribution of the amylopectin (Lloyd, Hedley, Bull, & Ring, 1996). The experimental evidence suggests that the newly discovered hard network contains crystals composed of amylosic chains, with chain lengths larger than those found for the branch-length distribution of normal wild-type amylopectin. We have proposed that this is a crystalline amylose network. However, in these mutant starches the distinction between amylose and amylopectin becomes less clear. It is possible that the hard network is formed from the so-called intermediate material, which may be variously described

as a lightly branched amylose or as a modified amylopectin containing more long chains. The important factor appears to be that these regions of the granule contain fine hard networks containing crystallites composed of amylosic chains longer in length than the branch lengths of the native amylopectin. The formation of crystals of amylosic chains of varying lengths within the matrix would affect the gelatinisation of the starch. The melting point of amylosic crystals depends on chain length (Moates, Noel, Parker, & Ring, 1997) and this could account for the broadened gelatinisation behaviour seen for the *rug5-a* mutant. The presence of an interconnected crystalline matrix (physical cross-linking) would inhibit swelling of the granule until the network structure melts at sufficiently high temperatures. The *rug5-a* mutation also causes an increase in the amount of B-type crystallinity within the granule.

The *rug5-a* mutant differs from the *r* mutant in that the fine, hard network is only observed in certain localized regions within the granule. This is not inconsistent with the heterogeneous distribution of crystalline material suggested by the light microscope pictures of *rug5-a* mutant starch granules imaged under crossed polarisers (Hedley et al., 2002). In the *r* mutant, the fine, hard network throughout the granule was considered to be brittle and likely to fail under osmotic or physical shock. This was used to explain the fissures and fracture of the granules. The partial distribution of the fine, hard network within *rug5-a* granules is consistent with the convoluted structure of the granule and might explain why these granules are not as fragile as the *r* mutant granules.

4. Conclusions

The present study, together with previous published work (Ridout et al., 2003, 2004), has used a set of isogenic pea mutants to examine how specific mutations in the starch biosynthetic pathway influence granule structure and functionality. We have found that mutations that lead to substantial changes in the amylose-amylopectin ratio lead to substantial changes in granule architecture and function. The four single mutants (*r*, *rug3*-a, *lam-c* and *rug5-a*) and the double mutant (*rrb*) all lead to detectable changes in granule ultrastructure. It has been proposed that these differences are largely associated with the amount, distribution and physical state of amylose within the granules. In the low-amylose mutants (*lam-c* and *rug3-a*), the reduction in the level of amylose does not significantly change the level of crystallinity within the granule. Selective swelling of the amorphous regions within the granule reveals a periodic banded (growth ring) structure, suggesting periodic variation in the structure of the granule. Both mutants contain similar low levels of amylose and in both cases it was not possible to visualise any blocklet structure within the granule, suggesting that the nature of the amorphous region of the granule has changed. This may mean that the distribution of crystalline lamellae within low-amylose starches is completely different to that found in the wild-type parent.

The wild-type parent and the substrate mutants *rb* and *rug4-b* contain similar levels of amylose. The blocklet structures observed in the AFM images of these samples are similar in size and shape. The blocklet size, shape and relative orientation is uniform throughout the granule. Blocklet structures as revealed by TEM (Gallant et al., 1997; Hood & Liboff, 1983) are clusters of crystalline lamellae (Fig. 1). At present the AFM studies cannot easily resolve individual crystal lamellae in unmodified materials. In the AFM, the blocklets are revealed by the selective swelling of the matrix material. The apparent blocklet size is determined by the periodic fluctuations in height within the image. This is strictly a measure of blocklet–blocklet separation and only provides an estimate of blocklet size. If the matrix material is mainly amylose, and the amylose contents are similar, then it is perhaps not surprising that the 'blocklet' shapes and sizes are similar.

In the high-amylose mutants (*r* and *rug5-a*), the level of crystallinity is largely unchanged but the amount of B-crystals increases to 100% (*r*) and 53% (*rug5-a*). In both mutants, we have identified the presence of fine, hard networks in the matrix region surrounding the blocklet structure within the granule. In the case of the *rug5-a* mutant, this structure is confined to certain regions of the granule and the granule structure is heterogeneous. This is consistent with the convoluted nature of the *rug5-a* granules. The continuous distribution of this fine, hard network throughout the *r* mutant granules has been used to explain the presence of fissures and fracture of the granules. The patchy nature of the hard network structure in the *rug5-a* granules may account for the less-fragile nature of these granules. The decrease in the amount of amylopectin in the granules without a significant drop in the level of crystallinity has been taken to suggest that some of the amylose may have crystallised in the matrix region surrounding the blocklets. This would account for the formation of the observed fine, hard network. There is strong circumstantial evidence in support of this assertion. The crystalline regions contain amylosic chains. In both the *r* and the *rug5-a* mutants, this chain profile contains an additional high molecular weight fraction not attributable to the conventional amylopectin structure found in the wild-type parent. The crystallisation of amylosic chains of varying lengths would lead to a spread in melting temperatures, and would account for the broadened gelatinisation behaviour of these mutants. The presence of such an amylosic network would influence the swelling of the granules and their subsequent processing. The differences in behaviour are attributed to the presence of a novel amylosic network. As discussed earlier this structure may arise from intermediate material produced within the granules, variously termed modified amylose or modified amylopectin. The present images and previous studies (Ridout et al., 2003, 2004) of the *r* mutant seem to indicate that the blocklet structures observed by AFM are larger and more elongated than those seen in the wild-type parent. In AFM images, the blocklets are revealed by selective swelling of the matrix material surrounding the blocklets. The force modulation AFM images of the *r* mutant suggest that this swelling is dominated by the fine, hard network within the matrix. Thus, the apparent observed changes in blocklet size and shape probably reflect the porosity of this network rather than any genuine change in

the number or distribution of crystalline lamellae. Interestingly, in the AFM images of the *rug5-a* mutant, in the regions where there is evidence for a fine, hard network structure in the matrix surrounding the blocklets, the apparent blocklet sizes are similar to those seen for the *r* mutant. In the regions where growth rings are present and no fine hard network is seen within the matrix, the apparent blocklet sizes are similar to those seen for the wild-type, *rb* and *rug4-b* samples.

Acknowledgements

The research described in this article was supported in part by the BBSRC core grant funding to the JIC and IFR and through funding from the EU Framework 4 FAIR (CT98-3527) programme. Apparatus used for the AFM studies was purchased through the award of a BBSRC Bioimaging grant, D11154. The authors wish to acknowledge useful discussions with Patrick Gunning and Steve Ring.

References

Baker, A. A., Miles, M. J., & Helbert, W. (2001). Internal structure of the starch granule revealed by AFM. *Carbohydrate Research*, *330*(2), 249–256.

Baldwin, P. M., Adler, A. J., Davies, M. C., & Melia, C. D. (1998). High resolution imaging of starch granule surfaces by atomic force microscopy. *Journal of Cereal Science*, *27*(3), 255–256.

Bogracheva, T. Y., Cairns, P., Noel, T. R., Hulleman, S., Wang, T. L., Morris, V. J., et al. (1999). The effect of mutant genes at the *r, rb, rug3, rug4, rug5 and lam* loci on the granular structure and physicochemical properties of pea seed starch. *Carbohydrate Polymers*, *39*(4), 303–314.

Bogracheva, T. Y., Davydova, N. I., Genin, Ya. V., & Hedley, C. L. (1995). Mutant genes at the *r* and *rb* loci affect the structure and physicochemical properties of pea seed starches. *Journal of Experimental Botany*, *46*(293), 1905–1913.

Bogracheva, T. Y., Morris, V. J., Ring, S. G., & Hedley, C. L. (1998). The granular structure of C-type pea starch and its role in gelatinisation. *Biopolymers*, *45*(4), 323–332.

Bogracheva, T. Y., Wang, Y. L., Wang, T. L., & Hedley, C. L. (2002). Structural studies of starches with different water contents. *Biopolymers*, *64*(5), 268–281.

Buleon, A., Colonna, P., Planchot, V., & Ball, S. (1998a,b). Starch granules: Structure and biosynthesis. *International Journal of Biological Macromolecules*, *23*(6), 85–112.

Cairns, P., Bogracheva, T. Y., Ring, S. G., Hedley, C. L., & Morris, V. J. (1997). Determination of the polymorphic composition of smooth pea starch. *Carbohydrate Polymers*, *32*(3–4), 275–282.

Denyer, K., Barber, L. R., Burton, R., Hedley, C. L., Hylton, C. M., Johnson, S., et al. (1995). The Isolation and characterization of novel-amylose mutants of *Pisum sativum* L. *Plant Cell and Environment*, *18*(9), 1019–1026.

Gallant, D. J., Bouchet, B., & Baldwin, P. M. (1997). Microscopy of starch: Evidence of a new level of granule organisation. *Carbohydrate Polymers*, *32*, 177–191.

Gernat, Ch., Radosta, S., Damaschun, G., & Schierbaum, F. (1990). Supramolecular structure of legume starches by X-ray scattering. *Starch/Stärke*, *42*(5), 175–178.

Harrison, C. J., Hedley, C. L., & Wang, T. L. (1998). Evidence that the *rug3* locus of pea (*Pisum sativum* L) encodes plastidial phosphoglucomutase confirms that the imported substrate for starch synthesis in pea amyloplasts is glucose-6-phosphate. *The Plant Journal*, *13*(6), 753–762.

Hedley, C. L., Bogracheva, T. Y., Lloyd, J. R., & Wang, T. L. (1996). Manipulation of starch composition and quality in peas. In G. R. Fenwick, T. Y. Hedley, J. R. Richardson, & S. Khoklhar (Eds.), *Agri-Food Quality 95. An interdisciplinary* (pp. 138–148). Cambridge: Royal Society of Chemistry.

Hedley, C. L., Bogracheva, T. Y., & Wang, T. L. (2002). A genetic approach to studying the morphology, structure and function of starch granules using pea as a model. *Starch/Stärke*, *54*, 235–242.

Hood, L. F., & Liboff, M. (1983). Starch ultrastructure. In D. B. Bechtel (Ed.), *New frontiers in food microstructure* (pp. 341–370). St Paul, MN: The American Association of Cereal Chemists, Inc.

Hylton, C., & Smith, A. M. (1992). The *rb* mutation of peas causes structural and regulatory changes in ADP glucose pyrophosphorylase from developing embryos. *Plant Physiology*, *99*(4), 1626–1634.

Lloyd, J. R., Hedley, C. L., Bull, V. J., & Ring, S. G. (1996). Determination of the effect of *r* and *rb* mutations on the structure of amylose and amylopectin in pea (*Pisum sativum* L). *Carbohydrate Polymers*, *29*(1), 45–49.

Moates, G. K., Noel, T. R., Parker, R., & Ring, S. G. (1997). The effect of chain length and solvent interactions on the dissolution of the B-type crystalline polymorph of amylose in water. *Carbohydrate Research*, *298*(4), 327–333.

Ohtani, T., Yoshino, T., Ushiki, T., Hagiwara, S., & Mackawa, T. (2000a). Structure of rice starch Granules in nanometre scale as revealed by atomic force microscopy. *Journal of Electron Microscopy*, *49*(3), 487–489.

Ohtani, T., Yoshino, T., Ushiki, T., Hagiwara, S., & Mackawa, T. (2000b). High resolution imaging of starch granule structure using atomic force microscopy. *Starch/Stärke*, *52*(5), 150–153.

Ridout, M. J., Gunning, A. P., Wilson, R. H., Parker, M. L., & Morris, V. (2002). Using AFM to image the internal structure of starch granules. *Carbohydate Polymers*, *50*(2), 123–132.

Ridout, M. J., Parker, M. L., Hedley, C. L., Bogracheva, T. Y., & Morris, V. J. (2003). Atomic force microscopy of pea starch granules: Granule architecture of wild-type parent, *r* and *rb* single mutants, and the *rrb* double mutant. *Carbohydrate Research*, *338*(20), 2135–2147.

Ridout, M. J., Parker, M. L., Hedley, C. L., Bogracheva, T. Y., & Morris, V. J. (2004). Atomic force microscopy of pea starch: Origins of image contrast. *Biomacromolecules*, *5*(4), 1519–1527.

Szymonska, J., & Krok, F. (2003). Potato starch granule nanostructure studied by high resolution non-contact AFM. *International Journal of Biological Macromolecules*, *33*(1–3), 1–7.

Szymonska, J., Krok, F., & Tomasik, P. (2000). Deep-freezing of potato starch. *International Journal of Biological Macromolecules*, *27*(4), 307–314.

Waigh, T. A., Kato, K. L., Donald, A. M., Gidley, M. J., & Reikel, M. J. 1. (2000). Side-chain liquid–crystalline model for starch. *Starch/Stärke*, *52*(12), 450–460.

Waigh, T. A., Perry, P., Reikel, C., Gidley, M. J., & Donald, A. M. (1998). Chiral side-chain liquid–crystalline polymeric properties of starch. *Macromolecules*, *31*(22), 7980–7984.

Wang, T. L., Barber, R. A., Denyer, K., Hedley, C. L., Hylton, C. M., Johnson, S., et al. (1994). Seed mutants in *Pisum*: *lam* (low amylose) a new locus affecting starch composition. *Pisum Genetics*, *26*, 39–40.

Wang, T. L., Bogracheva, T. Y., & Hedley, C. L. (1998). Starch: Simple as A, B, C? *Journal of Experimental Botany*, *49*(320), 481–502.